

Improved formulation of global QCD analysis
with zero-mass hard cross sections

Pavel M. Nadolsky^a, Wu-Ki Tung^{b,c}

^a Department of Physics, Southern Methodist University, Dallas, TX 75275, USA

^b Department of Physics and Astronomy, Michigan State University,
East Lansing, MI 48824, USA

^c Department of Physics, University of Washington, Seattle, WA 98105, USA

The zero-mass (ZM) parton formalism is widely used in high-energy physics because of its simplicity and historical importance, even while massive quarks (c, b, t) are playing an increasingly prominent role in particle phenomenology, including global QCD analyses of parton distributions based on the more precise general-mass (GM) QCD formalism. In view of this dichotomy, we show how the obvious inconsistencies of the conventional implementation of the ZM formalism can be corrected, while preserving the simplicity of its hard matrix elements. The resulting *intermediate-mass* (IM) scheme for perturbative QCD calculation can be considered either as *improved ZM formulation* with realistic treatment of heavy-flavor kinematics; or as a *simplified GM formulation* with approximate ZM hard cross sections. Phenomenologically, global analyses based on IM calculations can effectively reproduce, within the present estimated uncertainty bands, the more correct GM results on parton distributions, as well as their predictions for a wide range of collider processes of current interest.

PACS: 12.15.Ji, 12.38 Cy, 13.85.Qk

Contents

1	Introduction	2
2	Conventional ZM VFNS	3
3	Intermediate mass VFNS	6
3.1	Satisfying heavy-flavor production kinematics	6
3.2	Correct summation over physical final states	8
3.3	Comparison of calculational schemes with heavy-quark data	9
4	Global Analyses	11
4.1	Comparison of global fits in the ZM, IM and GM schemes	11
4.2	Comparison of parton distributions	12
4.3	Comparison of Physical Predictions	15
4.4	Generalized rescaling variable in the GM scheme	17
5	Concluding Remarks	17

1 Introduction

Global QCD analysis is based on factorization theorems of perturbative quantum chromodynamics (PQCD) at high energies. It allows the determination of universal parton distribution functions (PDFs) by comparing the QCD parton formulas with a wide range of available hard scattering data (which involve at least one large energy scale, generically referred to as Q). The conventional derivation of the factorization theorems in PQCD is formulated in the zero-quark-mass limit and is valid to $\mathcal{O}(\Lambda_{QCD}^2/Q^2)$ [1]. Since QCD interactions depend on the number of active quark flavors, and this number (denoted by n_f) varies in practice, it is necessary to vary n_f in the theoretical calculations according to the effective energy scale μ of the interaction—it is incremented by 1 every time μ crosses one of the mass thresholds for heavy quarks [2]. In the common implementation of this so-called variable-flavor-number-scheme (VFNS), the changes of n_f with the factorization scale across heavy-flavor thresholds are taken into account in the evolution of PDFs and in the summation over active parton flavors in the factorization formula, but heavy-quark mass effects are ignored in the hard matrix elements, as well as in the evaluation of the phase space of final states in the convolution integral. This provides a simple and convenient working platform for most calculations in high-energy phenomenology; and it has been widely used both in practical calculations and in global QCD analysis of PDFs. We shall refer to this calculational scheme as the *conventional* zero-mass (ZM) VFNS.

As the PQCD theory advanced, and the proper treatment of heavy quarks became more important, it was recognized that the validity of factorization ought to be extendable to PQCD with non-zero quark masses [3, 4], *i.e.* to be valid to order Λ_{QCD}^2/Q^2 uniformly, independent of the ratios m_h/Q of quark masses m_h for $h = c, b$, and t . This was formally proved for inclusive deep inelastic scattering in Ref. [5]. This generalized factorization, which does not assume $m_i/Q \rightarrow 0$ for all parton flavors i as in the ZM formalism, provides the basis for an improved global QCD analysis formulated in the general-mass variable-flavor-number scheme (GM VFNS). Recent GM VFNS global analyses [6–8] demonstrate that the proper treatment of heavy-quark mass terms is essential for reliable predictions of cross sections at the Tevatron and LHC. This is because a good fraction of input precision data from DIS and fixed-target experiments included in the global analysis are at energy scales comparable to, or not too far above, the charm and bottom masses [9]; hence the PDFs are sensitive to the more precise treatment of mass effects in the GM scheme.

Nonetheless, because the ZM PQCD formalism is much better known, and the requisite hard cross sections (Wilson coefficients) are much more readily available, the ZM VFNS remains ubiquitously used in particle physics applications, as well as in many contemporary global analyses of parton distributions [10–12]. With this in mind, it is useful to reexamine

the ZM calculations from a new perspective, to see whether it is possible to preserve its main simplifying feature, massless hard-scattering cross sections,¹ while correcting its other obvious inconsistencies. These inconsistencies, largely overlooked before, were recognized in [6]; the possibility of formulating improved implementation of the ZM scheme was raised in [9]. In this paper, we address this problem in detail. We are motivated by the observation that the differences between the GM and ZM PDFs that caused the observed shifts in the LHC W and Z cross section predictions arise mainly due to the kinematical suppression of heavy-flavor scattering cross sections near their respective mass thresholds in the global analysis. Inclusion of the correct kinematic treatment in the ZM global analysis can bring the resulting PDF's much closer to the GM analysis, while retaining the simplicity of the massless hard cross sections in the ZM scheme, if this is done with due care. We focus on the next-to-leading order (NLO) global analysis, which benefits most directly from such improvements.

In Section 2, we analyze the essential components of the variable flavor number scheme and identify those parts of the conventional ZM implementation that conflict with kinematic aspects of heavy-flavor production. Based on this analysis, in Section 3, we propose practical methods to correct these problems, leading to a class of “intermediate-mass” (IM) schemes that potentially can serve as effective approximations to the GM scheme. Numerical comparisons of ZM/IM/GM calculations are presented. In Section 4, we perform parallel global fits based on the ZM/IM/GM schemes, compare the effectiveness of the proposed IM schemes, and compare the PDFs and theoretical predictions for representative collider cross sections. Alternative choices of the rescaling variable in the GM scheme are considered in Section 4.4. Concluding remarks are given in Section 5.

2 Conventional ZM VFNS

The general PQCD factorization for high-energy hard processes, exemplified by the inclusive DIS structure functions $F_\lambda(x, Q^2)$, has the form

$$\begin{aligned} F_\lambda(x, Q^2) &= \sum_{a,b} \int_x^1 \frac{d\xi}{\xi} f_a(\xi, \mu) C_{b,\lambda}^a \left(\frac{\chi}{\xi}, \frac{Q}{\mu}, \frac{m_i}{\mu}, \alpha_s(\mu) \right) \\ &\equiv \sum_{a,b} [f_a \otimes C_{b,\lambda}^a] (\chi, Q, m_i, \mu). \end{aligned} \quad (1)$$

Here $f_a(\xi, \mu)$ is the parton distribution function for an initial-state parton a with momentum fraction ξ at the factorization scale μ , $C_{b,\lambda}^a$ are hard cross sections for the scattering of parton

¹It should be noted that ZM and GM hard cross sections are practically indistinguishable if the typical energy is much larger than m_c and m_b , as is the case in most collider phenomenology. In this high-energy regime, ZM hard cross sections are compatible with the PDFs obtained by global analyses in either mass scheme. What we are concerned here are the differences between the ZM and GM calculations at low Q that affect the global analysis of the precise DIS data from HERA at small x . The resulting differences in PDFs can affect predictions of physical observables at both low and high energies.

a into a final-state parton b , and m_i collectively represents the quark masses. The perturbatively calculable hard cross sections $C_{b,\lambda}^a$ are also variously known as Wilson coefficients, hard matrix elements, or, least formally, matrix elements. In VFNS, initial states a are summed over the active parton flavors at the factorization scale μ , typically chosen to be $\mu = Q$ (and equated here to the renormalization scale). The lower limit of the convolution integral χ is a function of the DIS kinematic variables (x, Q) determined by final-state phase-space constraints in each parton-level scattering subprocess.

In its general form, the factorization formula (1) applies both to the GM and ZM VFNS. With the insight gained from the modern formulation of the GM VFNS, we will now dissect this formula in the conventional implementation of the ZM formalism and expose the elements that are usually taken for granted together. (Since we always work with the VFNS in this paper, we shall omit the VFNS designation for both GM and ZM cases from now on.)

(i) **ZM hard matrix elements.** Central to the ZM formalism, the hard matrix elements in Eq. (1) are taken to be the standard ZM ones, $C_{b,\lambda}^a = C_{b,\lambda}^a \left(\frac{x}{\xi}, \frac{Q}{\mu}, 0, \alpha_s(\mu) \right)_{\overline{\text{MS}}}$: they are calculated under the assumption that all active partons are massless, with the associated singularities subtracted in the $\overline{\text{MS}}$ scheme. Their expressions are well-known—to NNLO in the QCD coupling $\alpha_s(\mu)$ for DIS and Drell-Yan processes [13], and to NLO for many other processes.

For the DIS process, the hard matrix elements are also known for non-zero quark masses to order α_s^2 [14], but the zero-mass formulas are much simpler and easier to use. Hence the ZM calculation is commonly used *because of its simplicity and convenience*. On the other hand, for almost all other physical processes, such as Drell-Yan pair, W/Z boson, and inclusive jet production, the GM hard matrix elements are not available beyond the leading order. Thus, *by necessity*, the ZM matrix elements are still widely used both in physical applications and in global analyses in general.

(ii) **Final-state counting.** The summation of the final-state parton flavors in Eq. (1), \sum_b , is conventionally taken to be over all active parton flavors at scale μ , the same as for the initial-state summation \sum_a .

This convention originated from the strict zero-mass parton formalism of the 1970's and 80's, but is clearly problematic from the modern perspective. As emphasized in [6, 9], there is an important conceptual difference between the initial- and final-state summations \sum_a and \sum_b . \sum_a runs over the active parton flavors, a *theoretical* concept dependent on the choice of the renormalization scheme for α_s , the factorization scheme for the PDFs, and, of course, the value of μ . On the other hand, \sum_b involves summation over *physical* final states that are kinematically allowed at the given scattering energy. Determined by *physical* kinematical considerations, \sum_b should be *independent* of the choice of the renormalization and factorization schemes and the scale variable μ .

This dichotomy leads to unintended inconsistencies for the conventional ZM calculation. For example, consider a small- x kinematic configuration common at HERA, say $x = 10^{-4}$

and $Q = 3$ GeV, corresponding to virtual Compton scattering center-of-mass (CM) energy $W = Q \sqrt{x^{-1} - 1} = 300$ GeV. Because the factorization scale $\mu = Q = 3$ GeV is smaller than the bottom quark mass m_b , the bottom quark b in this calculational scheme is not counted as an active parton; thus the final-state parton flavor summation does not include b . However, in reality bottom quarks are easily produced at this CM energy W , as is indeed experimentally observed. The problem is even more pronounced for Q around and below the charm mass m_c .

(iii) **Phase-space treatment.** In ZM calculations, the convolution integral $\int_\chi^1 \frac{d\xi}{\xi}$ in Eq. (1) is usually computed using massless parton kinematics, so that χ in the lower integration limit is equated to the Bjorken $x = Q^2/(2q \cdot p)$. For the leading-order quark scattering process $V^*a \rightarrow b$ (where V^* stands for the virtual vector boson $\gamma^*/W/Z$), this leads to the well-known result $F_\lambda(x, Q^2) = \sum_{a,b} C_{b,\lambda}^a f_a(x, Q)$, where $C_{b,\lambda}^a$ are the appropriate (electroweak) coupling parameters.

Because this integral originates from summing over final-state phase space of *real* particles, this practice leads to violation of Lorentz kinematics in the case of heavy-flavor production. For instance, in neutral-current DIS at $Q \gtrsim m_b$ and $W \lesssim 2m_b$ (say, $x \sim 0.3$), this calculational scheme will predict similar contributions from b quark production and d sea quark production (since ZM hard matrix elements are flavor-independent), whereas, in fact, this kinematical regime is below the b -production threshold, and the b and d scattering cross sections are completely different!

Past global QCD analyses carried out in the ZM scheme have overlooked these unphysical features, since the heavy-quark contributions to flavor-inclusive cross sections are relatively small. The resulting deviations from the true behavior are compensated in the global analysis process by the fitting process, leading to very good agreement with the examined data. Thus, many ZM PDFs (including CTEQ6 [10] and CTEQ6.1 [11]) have been widely used in comparisons of current experimental measurements to theory, and in making predictions for new processes in collider phenomenology.²

Having identified the unphysical features of the conventional implementation of the ZM scheme in this section, we can now investigate whether these elements can be corrected, while preserving its simple matrix elements, to produce a simple and effective approximation to the GM theory. This is worthwhile, since the ZM formalism is very versatile and practicable; and it is still used in the vast majority of applications.

²Parallel PDF sets in the GM VFNS, such as CTEQ5HQ/CTEQ6HQ [15, 16], were also provided along with CTEQ6 and CTEQ6.1. They have not been used as widely in general applications, but served as standard PDFs in the analysis of heavy-quark production.

3 Intermediate mass VFNS

From the presentation of the last section, we can see that the particulars of counting final states and of treating final state phase space in the conventional implementation of the ZM scheme (points (ii) and (iii) of the previous section) are not intrinsic to the ZM treatment of hard matrix elements (point (i)). With the insight gained from the GM formulation of [6], we can try to eliminate these kinematic contradictions on inclusive cross section calculation from the ZM scheme. There is no unique way to do this, even though the underlying physics provides valuable guidance on how to proceed. We shall now discuss the possibilities.

3.1 Satisfying heavy-flavor production kinematics

First, consider the issue of **phase space integration** for a given partonic subprocess contributing to the right-hand side of Eq. (1), say the LO $V^* + q \rightarrow h$, where q denotes either a light or heavy quark, and h a heavy quark (c, b, t). In the conventional implementation of ZM, for zero-mass kinematics, one gets the contribution $F_\lambda(x, Q^2) = C_{h,\lambda}^q f_q(x, Q)$, which runs into serious problems if W is near or below the production threshold for the heavy quark. It has been known since early days of charged-current DIS [17], and, more recently, from the GM approach [6, 9, 18] that the phase space constraint due to heavy-quark masses can be naturally implemented by replacing the Bjorken x above by a *rescaling variable* “ACOT- χ ”,

$$\chi = x \left(1 + M_f^2/Q^2\right), \quad (2)$$

where M_f denotes the total mass of the final state (m_h for charged-current DIS, $2m_h$ for neutral-current DIS), *i.e.* $F_\lambda(x, Q^2) = C_{h,\lambda}^{q,(0)} f_q(\chi(x, Q), Q)$. One can easily verify that, as W approaches the heavy-quark production threshold M_f from above, $\chi \rightarrow 1$; thus $F_\lambda \rightarrow 0$ in the heavy-quark production channel, as it should.³

This problem is general, applicable also to NLO and beyond: by extending the lower bound of the convolution integral to Bjorken x in Eq. (1), the conventional ZM formalism grossly overestimates the contributions from the region of phase space near (and even beyond) the physical thresholds *for all channels*. A straightforward way to correct this problem is to replace the lower limits of the convolution integral with the equivalent rescaling variable $\chi(x, Q)$ for all terms. This would restrict the phase space to the physically allowed region, and, importantly, also ensure consistency between the LO and higher-order terms with respect to a shift of the factorization scale. However, this prescription is not unique; and it needs some careful consideration. For instance, the rescaling prescription Eq. (2) involves an upward shift of the variable x by a constant factor $(1 + M_f^2/Q^2)$, even though the physical mass-threshold kinematic constraint is mainly a large- x (low- W) issue for a given Q . Since parton distributions are rapidly varying functions at small x , the suppression of phase space

³This rescaling is more than just a convenient prescription. Its emergence can also be seen in the origin of the LO term as the resummation of collinear singularities of higher order terms in the limit $Q \gg M_f$: if mass effects are kept, this variable will appear naturally in the collinear terms, cf. [18].

due to the substitution $x \rightarrow \chi$ could unnecessarily suppress the contribution from the gluon fusion term in the small- x region, causing potential disagreement with the accurate DIS data from HERA.

It is therefore desirable to generalize the rescaling variable χ , so that it enforces the mass-threshold constraint at large x in the same natural way, but smoothly recovers the standard scaling x variable away from the mass threshold (*i.e.*, at small x) in a controllable way. We introduce a new rescaling variable ζ using the relation, modeled after Eq.(2):

$$x = \zeta \left(1 + \zeta^\lambda M_f^2/Q^2\right)^{-1}, \quad (3)$$

where the parameter λ is a positive number. The variable ζ has the following properties:

- a) it reduces to Bjorken x for large Q ($\zeta \rightarrow x$ as $Q \gg M_f$), and the $\zeta \rightarrow 1$ limit corresponds to the physical mass threshold ($W \rightarrow M_f$)—both key features of a rescaling variable;⁴
- b) for non-zero λ , the rescaling effect is reduced as x moves toward smaller values, away from the threshold region where it is required; and
- c) for a given Q , $x < \zeta < \chi$, *i.e.* ζ lies in-between the ZM x (which violates non-zero mass kinematics) and the uniform rescaling variable χ (which may be too restrictive).

The rescaling factor ζ/x is shown in Fig. 1 for several values of λ . The top horizontal line, $\lambda = 0$, corresponds to uniform rescaling $\zeta = \chi$. The base line corresponds to the ZM case $\zeta = x$. Those two lines are parallel, since χ/x is a constant factor, as already mentioned. The other curves correspond to $\lambda = 0.1, 0.2$, and 1 , respectively. The amount of suppression of phase space away from the physical mass threshold can be controlled in a smooth way by varying the parameter λ . The small- x rescaling is reduced for increasing values of λ ; and it has practically vanished below $x = 0.1$ even for a moderate choice of $\lambda = 1$.⁵ The range of variation of the rescaling variable, represented by the width between the two horizontal lines, is M_f^2/Q^2 ; it shrinks rapidly for increasing values of Q . Thus, *rescaling at high energy scales is negligible for any choice of λ for all x .*

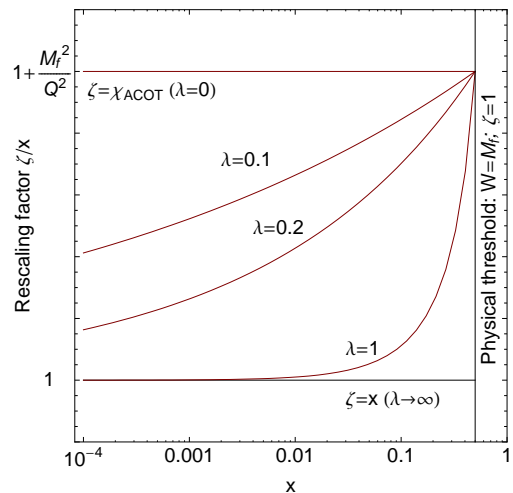


Figure 1: The rescaling factor ζ/x vs. x for $\lambda = 0, 0.1, 0.2$, and 1 .

The rescaling variable ζ is simple and flexible. It can be used effectively to explore how well the conventional ZM formulation can be improved to yield more reliable predictions. In the next section, we will show examples of global fits based on improved ZM calculations with this variable, with selected values of the parameter λ . We will find that the generalized rescaling variable is the key requisite needed to correct the kinematical dependence of the ZM cross sections, while the other modifications (discussed in the next subsection) play a secondary role.

⁴Specifically, one can show that $W^2 = Q^2 \left((1 + \zeta^\lambda M_f^2/Q^2) \zeta^{-1} - 1 \right)$, neglecting ordinary hadron masses.

⁵The limiting case $\zeta = x$ is reached in Eq.(3) formally by taking $\lambda \rightarrow \infty$. But, as can be seen from the steep rise of the rescaling factor curves for larger values of λ in Fig. 1, the transformation as $x \rightarrow 1$ is ill-defined in this limit. For all practical purposes, $\lambda \approx 1$ already produces enough small- x suppression of rescaling to produce results close to that using directly $\zeta = x$, while ensuring kinematic bounds.

3.2 Correct summation over physical final states

Next, we turn to the issue of **summation over final-state partons**, \sum_b of Eq.(1)—point (ii) raised in Sec.2. This is intimately related to the choice of partonic subprocesses included in the calculation for the given combination of kinematical parameters. Consider, in particular, production of a b quark in neutral-current DIS discussed in item (ii) of the previous section ($x \sim 10^{-4}$, $Q \sim 3$ GeV, $W \sim 300$ GeV). Since $b\bar{b}$ pairs are physically produced in the final state, the gluon fusion subprocess $\gamma^*g \rightarrow b\bar{b}$ must be included in the sum of non-zero scattering contributions independently of the choice of the factorization scheme and scale. In the conventional implementation of the ZM scheme, with the scale $\mu = Q = 3$ GeV being below the bottom mass, this subprocess is not included, resulting in the dilemma mentioned in Sec.2. But, there is no reason, in principle, to tie the final-state parton summation \sum_b to the initial-state one, \sum_a . In fact, in the fixed-flavor-number scheme, as in the GM VFNS, the subprocesses $\gamma^*g \rightarrow c\bar{c}$, $b\bar{b}$ are always present whenever there is enough CM energy to produce these heavy-flavor states. Therefore, we can try to adopt the same physically sensible approach in the ZM scheme, i.e. we shall include these subprocesses while keeping the ZM hard matrix elements.

However, this seemingly straightforward “fix” of the conventional implementation of ZM is not entirely trivial. The ZM matrix element for the partonic subprocess $\gamma^*g \rightarrow b\bar{b}$ is obtained after a subtraction,

$$C_{b,\lambda}^g(\mu) = C_{b,\lambda}^g(1/\varepsilon)_{\text{unsubtracted}} - \overline{\text{MS}} \text{subtraction}(1/\varepsilon, \mu), \quad (4)$$

where the subtraction term represents the collinear singularity due to the zero quark mass approximation. This term is sensitive to μ , and in general its μ dependence matches that of the PDF $b(x, \mu)$ in the LO $\gamma^*b \rightarrow b$ term. If this LO term is absent because of the conventional scale choice $\mu = Q$ while $Q < m_b$, there would be a mismatch; then the simple addition of the $\gamma^*g \rightarrow b\bar{b}$ subprocess, using Eq.(4), would be incorrect. However, this problem arises only because of the choice of the default scale $\mu = Q$, not because of the ZM formalism itself. For heavy-flavor production, it is in any case natural to choose a factorization scale $\mu > m_b$, e.g. $\mu = \sqrt{Q^2 + m_b^2}$. Then the corresponding LO will be present, and consistency is restored. Clearly, any choice of μ that stays above m_b and approaches Q at high energies would be equally acceptable. The differences will be of higher order. We have verified that the results are not sensitive to the scale choice, hence will use the above as the default.

There are also other ways of compensating for the $\overline{\text{MS}}$ subtraction to the gluon-fusion contribution if the LO processes $\gamma^*b \rightarrow b$ and $\gamma^*\bar{b} \rightarrow \bar{b}$ are absent. For instance, in the GM calculation, the term that removes the collinear singularity of the unsubtracted gluon fusion term is [4],

$$\frac{\alpha_s}{2\pi} \ln \left(\frac{\mu^2}{m_b^2} \right) \left[C_{b,\lambda}^{b(0)} \otimes P_{qg} \otimes f_g \right] \quad (5)$$

where f_g is the gluon distribution, P_{qg} is the $g \rightarrow q$ splitting function, and $C_{b,\lambda}^{b(0)}$ is the LO ZM matrix element for $\gamma^*b \rightarrow b$ contribution to the structure function F_λ . This logarithmic term

is equivalent to the subtraction term in Eq. (4), cf. [4]. Therefore, one can consider adding (5) to the ZM matrix element $C_{b,\lambda}^g(\mu)$ in order to maintain consistency (scale independence).⁶

The modified formulations of the ZM described in the above two subsections are designed to remedy the obvious problems of the conventional ZM in both the (large x , small W) and the (small x , small Q) regions, as identified in Sec. 2. They illustrate the point that the simplicity of the ZM parton formalism can be retained without the manifest violation of physical requirements. The proposed modifications of the conventional implementation are not unique. The differences between the modified choices all vanish at energy scales much larger than m_h ; and they usually are one order higher in α_s .

These improvements are all motivated by, and adapted from, recent implementations of the more accurate GM formalism [6, 9]. They belong to an intermediate stage between the ZM and the GM formalisms, hence will be designated as *intermediate-mass variable flavor number schemes* (IM VFNS, or IM scheme). They can be viewed either as improved ZM calculations with physical treatment of final states inspired by GM, or equivalently, as simplified GM calculations with suitably defined ZM hard cross sections.

3.3 Comparison of calculational schemes with heavy-quark data

To carry out a comparative study, we have implemented the conventional ZM and the various formulations of the IM scheme described above in our CTEQ global analysis program, alongside with the existing implementation of the GM scheme that by now has become the standard.

As a first step, we compare the heavy-quark calculational schemes by evaluating inclusive DIS cross sections with heavy quarks in the final state, using known PDFs. These cross sections are most directly affected by the heavy-quark mass treatment, hence give us a clear measure of the significance of the various calculational schemes. The data sets consist of charm production from H1 [19–21], ZEUS [22, 23], CCFR and NuTeV [24]; and bottom production from H1 [20, 21]. The total number of data points is 222.

For this initial comparison, the cross sections are calculated in the conventional ZM formulation, the GM formulation, and the IM formulation of Sec. 3.2. For each of these calculations, we first evaluate the cross sections using the PDFs of the latest GM global fit CTEQ6.6M [7] (abbreviated as CT66). These numbers are useful as references for assessing the results. The other PDF set used for comparison is CTEQ6.1M [11] (abbreviated as CT61), which represents the latest CTEQ ZM PDF set (2003).⁷ The χ^2 values for each combination of the calculational scheme and PDF set serve as a measure of the goodness-of-

⁶Since $f_b \approx \frac{\alpha_s}{2\pi} \ln(\frac{\mu^2}{m_b^2})[P_{qg} \otimes f_g]$ in the $\mu \sim m_b$ region, this term is essentially the same as the (absent) LO term $[C_{b,\lambda}^{b(0)} \otimes f_b]$. Thus, the underlying physics is similar to that of the default of the previous paragraph, and the effect on the results turns out to be similar, too, cf. Sec. 4.2.

⁷The original CT61 analysis did not include the latest data sets for semi-inclusive DIS heavy-quark production. The effect of including the newest heavy-quark data on the ZM PDFs will be described in the comparisons presented below.

fit in the comparison of theory with data. They are presented graphically in Fig. 2. In the two IM calculations, we adjust the parameter λ in the rescaling variable ζ of Eq. (3) so as to obtain the lowest possible χ^2 with the heavy-quark data for each examined PDF set.

* The GM calculation using CT66 (leftmost bar) agrees perfectly with the experimental data— χ^2 of 186 for 222 data points. The dashed line, corresponding to $\chi^2/\text{point} = 1$, is drawn for reference.

* The ZM calculation using CT66 PDFs (second to rightmost bar) fails dramatically compared to data by comparison. Since the CT66 PDFs, as far as we know, are the closest to the true PDFs, the ZM-CT66 column gives a reasonable measure of the size of the error of the ZM calculation in the conventional implementation— $\chi^2 \sim 1200/222$ points—a very large discrepancy. The same point is illustrated by the GM-CT61 column (second leftmost). In this case, since the GM scheme comes closest to the correct calculation, the discrepancy provides an approximate measure of how the CT61 PDFs are distorted to compensate for the imperfect calculation used in the original ZM fit.

* The χ^2 value is the largest in the case of the ZM-CT61 calculation. This discrepancy is partially accounted for by the fact that the heavy-quark data did not exist at the time of the CT61 global analysis. This number comes down to $\chi^2 = 406$ if the recent heavy-quark data are included (by performing an updated ZM analysis), as shown by the darker-colored part of the ZM-CT61 bar. But the updated CT61 PDFs still do not achieve the level of agreement with the data observed in the GM-CT66 calculation, as can be observed from the comparison of the leftmost (GM-CT66) and rightmost (ZM-CT61) bars in the figure.

* The impact of the IM scheme is illustrated by the IM-CT66 calculation. We chose $\lambda = 0.05$ in the rescaling variable ζ so as to attain the lowest χ^2 with the examined heavy-quark data sample. The IM scheme dramatically reduced the ZM-CT66 mismatch, with χ^2 decreased from 1240 to 337. Corrective measures adopted in the IM formulation, addressing manifest flaws of the conventional ZM treatment, do have a decisive, positive effect. The IM-CT61 fit similarly performs better than ZM-CT61, resulting in the reduction of χ^2 to 347, reached for $\lambda = 0.22$.⁸

These results provide an incentive to pursue a more detailed study of the IM formulation, including a new global fit of PDF's in this formulation. Since these calculations retain the

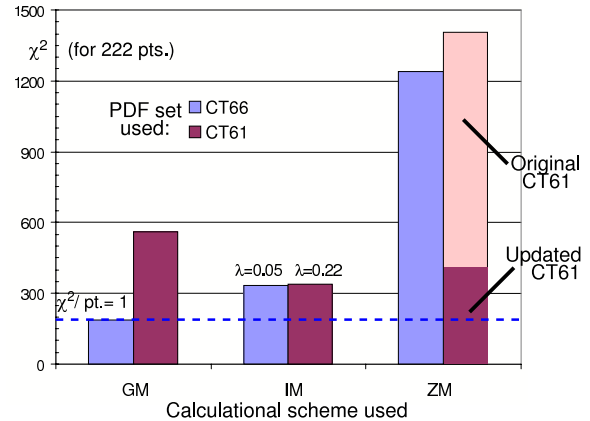


Figure 2: The log-likelihood χ^2 for 222 data points from neutral- and charged-current heavy quark semi-inclusive DIS, obtained in the GM, IM, and ZM schemes.

⁸The original ACOT rescaling variable χ (defined in Eq. (2) and equivalent to the variable ζ with $\lambda = 0$) produces worse IM fits, with the log-likelihood $\chi^2 = 354$ in the CT66 case and 650 in the CT61 case.

zero-mass matrix elements, they are still only approximations to the GM scheme. What we have seen here is that, in practice, the numerical effects due to the final-state counting and phase space treatment (that have been corrected) are larger than those due to the approximate hard matrix elements (that remain). Thus, it is possible that the core feature of the ZM scheme—its simple hard matrix elements—can be preserved in a viable global analysis.

4 Global Analyses

We now turn to the comparison of global analyses performed using the various schemes. The goal is to quantitatively study how the proposed IM schemes bridge the gap between the GM scheme (CT66) and the conventional ZM (CT61 and its updated equivalent). We will explore in detail the efficacy of several realizations of IM scheme described in Sec. 3, by comparing both the parton distributions and the physical predictions of complete global analyses based on these realizations with those of the conventional ZM and the GM formulations.

4.1 Comparison of global fits in the ZM, IM and GM schemes

We found that among the possibilities explored, the choice of the rescaling variable (Sec. 3.1) has the largest impact. We present here results from four IM global fits, for $\lambda = 0.3, 0.15, 0.05$, and 0 in the rescaling variable ζ defined in Eq. (3). These fits are identified as IMa, IMb, IMc, and IM χ . The conventional ZM fit (denoted as ZM0) is close numerically to all IM fits with $\lambda \gtrsim 1$. All these fits use the same experimental input data and parametrizations of the input nonperturbative PDFs as in the reference CT66 fit (denoted by GM) [7], in order to allow meaningful comparisons.

The goodness-of-fit χ^2 values in these global fits are shown in Fig. 3. For a total of 2716 data points, the best fit is given by the reference GM fit CT66 ($\chi^2 = 2760$). This is physically significant—the GM QCD formalism is in better agreement with a wide variety of global data than all the approximate ZM and IM formulations. The quality of the IM fits shows sensitive dependence on the value of the λ parameter that controls the rescaling behavior. The χ^2 ’s of the two worst fits, ZM0⁹ and IM χ at the

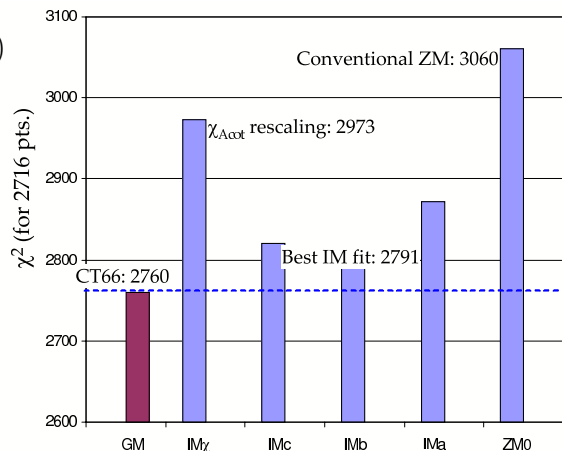


Figure 3: The global χ^2 values obtained in the GM, IM, and ZM0 schemes discussed in the text.

⁹The ZM0 fit is similar, but not identical, to the earlier CTEQ6.1 fit [11], cf. footnote 7. The results of this ZM fit were used in obtaining the “updated CT61” column of Fig. 2.

upper and lower ends of this group, are ~ 300 higher than in the reference fit (for 2716 data points)—beyond the acceptable range of fits characterized by the 90% C.L. criterion of CTEQ analyses ($\sim \Delta\chi^2 \lesssim 100$ [6, 7, 10, 11]). In between these two special cases, the quality of the global fit spans a continuous range, with the best fits to the global data occurring for the λ parameter around 0.15. The IMb fit ($\lambda = 0.15$) has an overall χ^2 of 2791—only 31 above that of the CT66 fit. It provides reasonable description of the heavy-quark SIDIS data examined in Section 3.3, with $\chi^2 = 212$ for 222 data points. By these criteria, it is well within the usual range of acceptable fits.

All the new IM global fits shown in Fig. 3 use the default prescription for treating heavy-flavor final states described in Sec. 3.2. As pointed out there, one can alternatively choose either a different scale (other than the default $\mu = \sqrt{Q^2 + m_h^2}$), or a different way of compensating the $\overline{\text{MS}}$ subtraction in the ZM gluon-fusion matrix element. We have investigated the effects due to both of these options on the global fit. They turn out to be relatively small compared to those of varying λ described above: the overall χ^2 of the global fit does not change by more than ~ 15 for all reasonable alternative choices in either cases (for any given λ).

Since the IM calculations still retain the ZM hard matrix elements, the IM PDFs will involve some adjustments made to compensate for this approximation. We shall try to quantify the deviations of the PDFs of these global fits from those of the GM reference fit, as well as the possible differences in their predictions in the next section. (We shall find both to be surprisingly small for the best IM fits.)

4.2 Comparison of parton distributions

Poor χ^2 values in the bad fits (ZM0 and IM χ) from the previous section are caused, for the most part, by disagreements with the high-precision HERA data points at small x and small Q . This is expected, in view of the problems of the ZM scheme and the conventional rescaling variable χ at small x discussed in Sections 2 and 3. To gain more insight on this, we show in Figs. 4 and 5 the u -quark and the gluon distributions of the ZM0/IMb/IM χ analyses, normalized to those of the standard fit CT66M, at two scales, $Q = 2$ GeV and 85 GeV. The d -quark distribution behaves in a similar way as for the u -quark (only with larger error bands), hence is not separately shown. The radiatively generated charm and bottom PDFs (not shown either) behave similarly to the gluon PDFs. To provide a useful reference for gauging the size of the deviations, we also show the uncertainty bands of the CT66 PDFs that result from the propagation of the input experimental uncertainties.

We see that the ZM0 and IM χ PDFs lie on opposite sides of the CT66 PDFs; and the PDFs of the best IM fit, IMb, lie in between. The quark distributions of the ZM0 set are suppressed compared to those of CT66, particularly at small x . This is because, with no threshold mass suppression or rescaling in the ZM0 fit, the magnitude of the heavy-quark scattering contributions to inclusive DIS structure functions is overestimated (especially at small x), resulting in suppressed light-flavor PDFs in order to compensate for excessive heavy-quark scattering in the global fit [6, 7]. On the other hand, χ rescaling introduces too

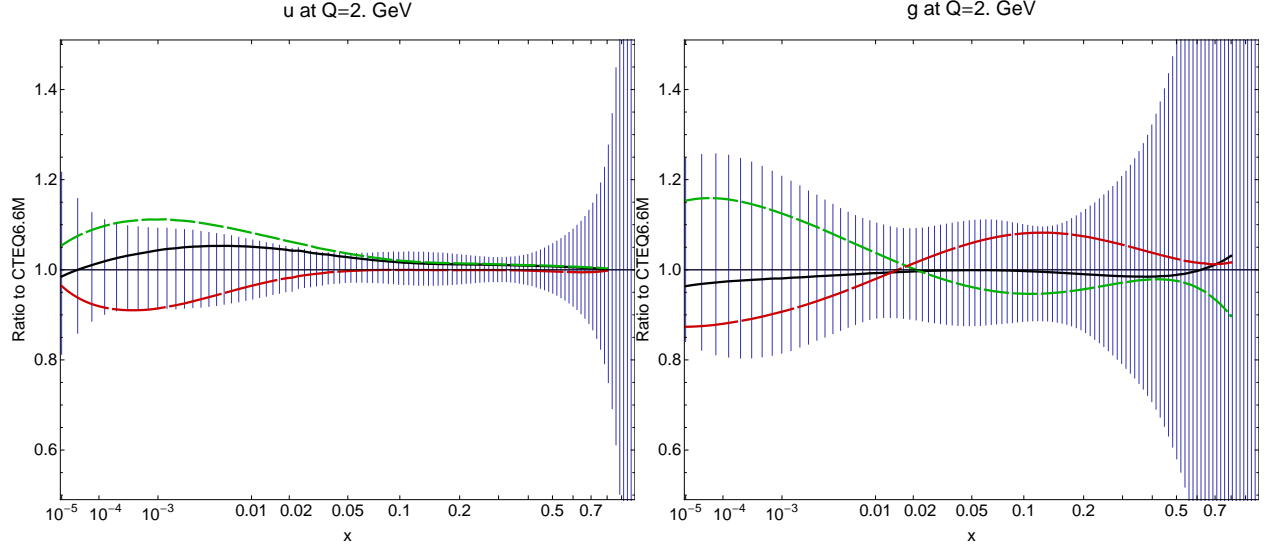


Figure 4: The x dependence of the u -quark (left) and gluon (right) PDFs at $Q = 2$ GeV, plotted as ratios to the CTEQ6.6M u -quark and gluon PDFs. The blue band is the CTEQ6.6 PDF uncertainty. The lines correspond to IMb (black solid), ZM0 (red long-dashed), and IM χ (green short-dashed) PDFs.

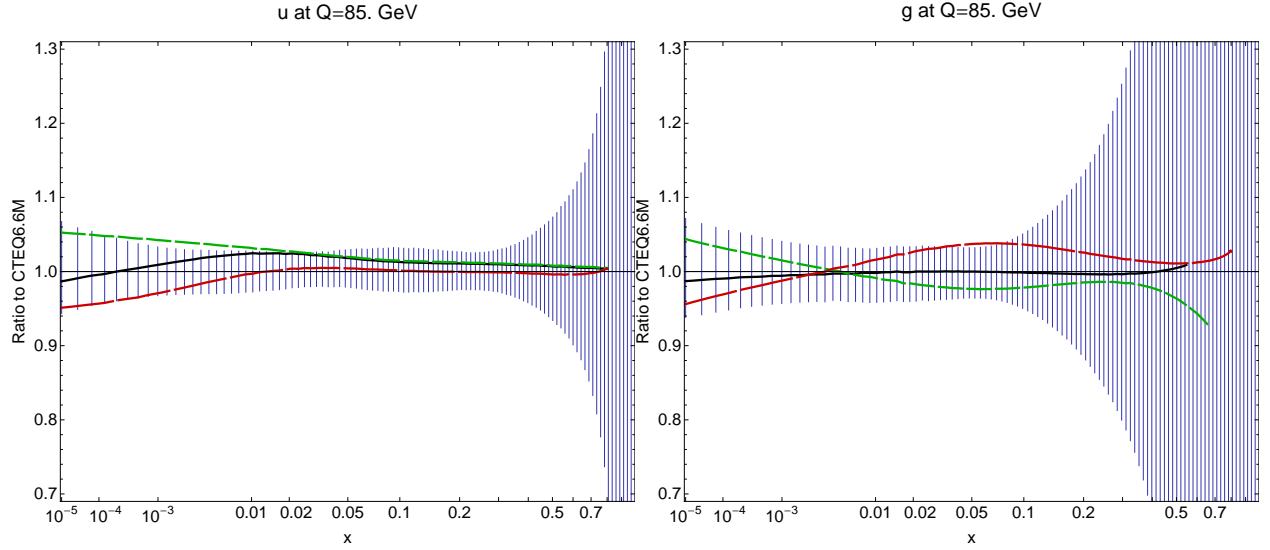


Figure 5: Same as Fig. 4, at $Q = 85$ GeV.

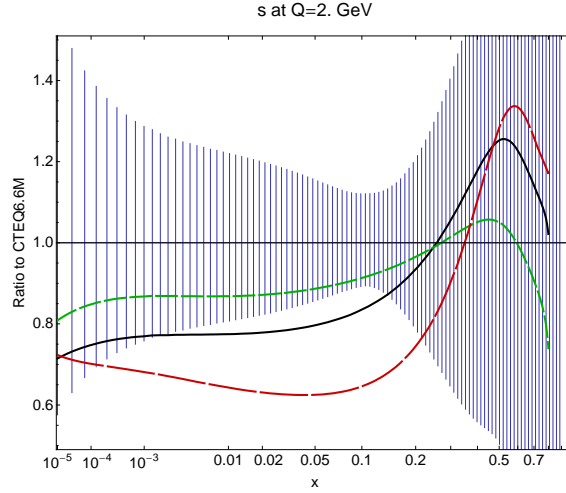


Figure 6: Same as in Fig. 4, for the strange quark PDF at $Q = 2$ GeV.

much suppression of phase space in heavy-quark DIS contributions at small x (cf. Sec. 3.1), resulting in overcompensated light-flavor PDFs. The gluon distribution shows similar suppression/enhancement as the quark distribution at small x , but this behavior reverses itself at moderate values of x —mostly as a consequence of the momentum sum rule constraint.

For both ZM0 and IM χ fits, the deviations of the light quark distributions from their CTEQ66 counterparts at small x are at the boundary of the PDF uncertainty bands; whereas those of the g , c , and b distributions stay generally within the bands. With the rescaling effect operative at large x (where it is well motivated), but suppressed at small x (where it is not necessarily needed on physical ground), the intermediate fit, IMb, yields the PDFs in-between the two extreme cases. The u and d (anti)quark PDFs in the IM scheme are consequently closer to the CT66 reference PDFs (surprisingly so for the gluon). The rescaling variable ζ adopted in Section 3.1 is thus capable of bringing both the global χ^2 value and shapes of the majority of the PDFs in the IM analysis close to those in the full GM scheme.

The strange-quark PDFs $s(x, Q)$, shown in Fig. 6, look more different than the other flavors. In global analysis, $s(x, Q)$ is not as well constrained in general because it is only sensitive to data on charm production in neutrino scattering, which is not very precise. The IM χ PDF is in better agreement with the CTEQ6.6 PDF than the IMb one, suggesting that the charged-current cross sections prefer a smaller value of λ (i.e., closer to ACOT χ) than the overall value of 0.15 for the best fit. (The rescaling variable ζ has different mass dependence in the two cases.)

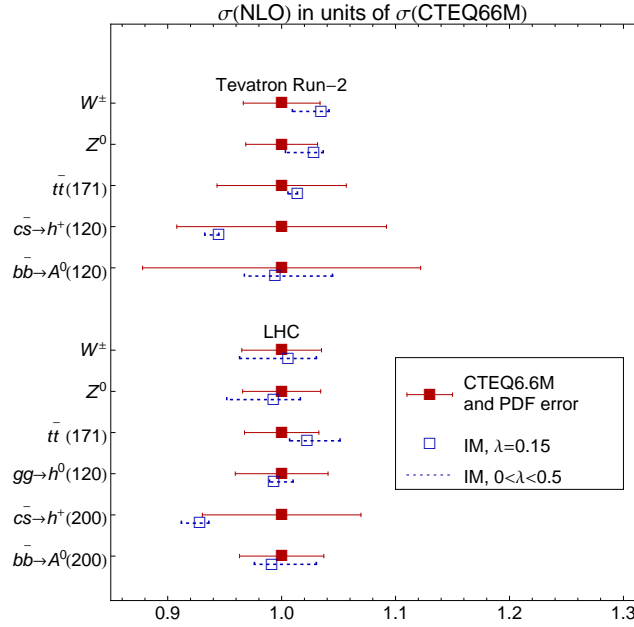


Figure 7: Representative NLO cross sections at the Tevatron and LHC, normalized to the CTEQ6.6M cross sections.

4.3 Comparison of Physical Predictions

To see how well the IM PDFs do in high-energy physics phenomenology, we have compared theoretical total cross sections for a number of representative scattering processes at the Tevatron and the LHC using the new PDF sets described above. In this calculation, we adopted the procedure of the analogous comparison in the CTEQ6.6 paper [7]. To probe typical combinations of parton distributions and x values, we show cross sections for production of W^\pm and Z^0 bosons; top quark-antiquark pairs (for top quark mass $m_t = 171$ GeV); Standard Model Higgs bosons h^0 with mass 120 GeV in gg fusion [25, and references therein]; supersymmetric neutral CP-odd Higgs bosons A^0 with masses 120 and 200 GeV in $b\bar{b}$ annihilation [26]; and supersymmetric charged Higgs bosons h^\pm in $c\bar{s}$ scattering [27]. Details of these calculations are provided in Section 4 of Ref. [7]. The cross sections are evaluated at the next-to-leading-order in the QCD coupling strength α_s using the program WTTOT [28].

Fig. 7 compares the IM and CTEQ6.6 total cross sections. The central predictions (denoted by boxes) correspond to the best-fit CTEQ6.6 and IMb PDF sets. Filled red boxes and error bars denote the CTEQ6.6 predictions and the PDF errors due to the propagation of experimental uncertainties. Empty blue boxes are for the best-fit IM fit with $\lambda = 0.15$; the dashed lines represent the range of IM predictions for the rescaling parameter λ in the range $0 \leq \lambda \leq 0.5$. We see that the IMb central predictions, and the IM ranges, mostly lie within the CTEQ6.6 PDF uncertainty bands. The IM calculational scheme is thus able to reproduce general features of a variety of GM cross sections. The only exception seen, for

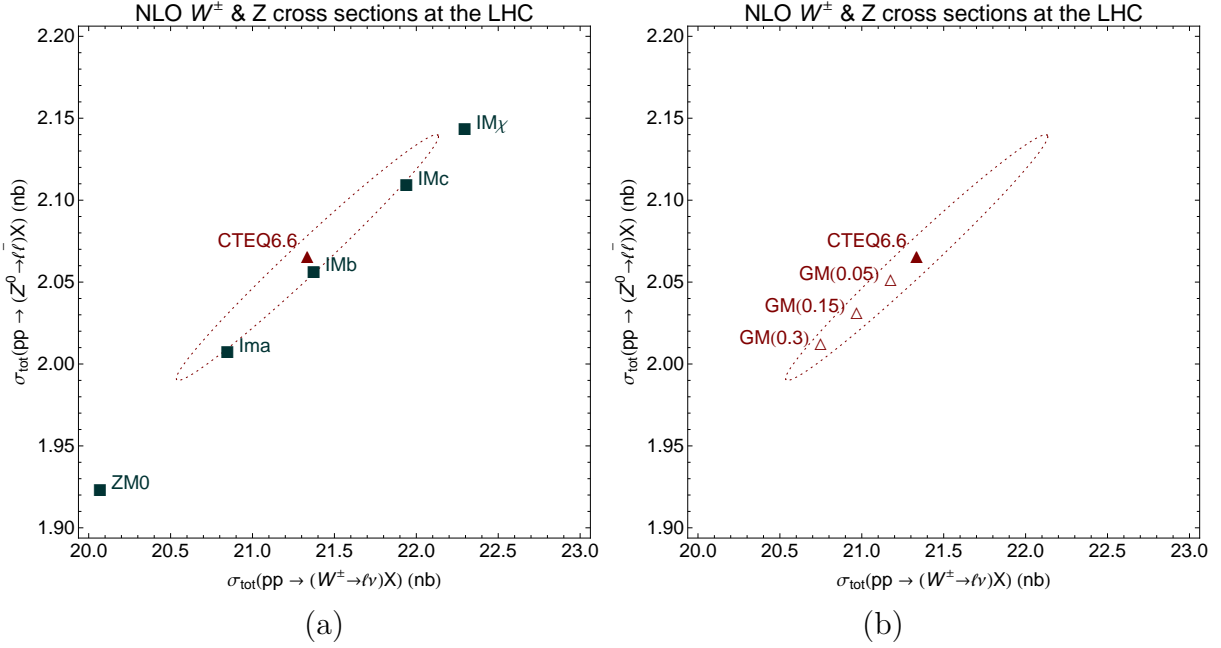


Figure 8: NLO W^\pm and Z production cross sections at the LHC, for CTEQ6.6M and the respective PDF uncertainty (red triangle and dashed ellipse); for best-fit ZM0, Ima, IMb, IMc, and IM χ PDFs (left subfigure, filled blue boxes); for GM fits with $\lambda = 0.05, 0.15, 0.3$ (right subfigure, empty red triangles).

$c\bar{s} \rightarrow h^+$ at the LHC, is due to the strange quark as mentioned at the end of Section 4.2.

The IM results for W and Z production cross sections at the LHC are shown in the two-dimensional plot of Fig. 8(a). The ellipse in the plot corresponds to the CTEQ6.6 PDF uncertainty range, similar to the bands shown in the previous figure. We see that the ZM0 and IM χ predictions are far away from the CTEQ6.6M one, in opposite directions; while the intermediate ones are close to the boundary of the uncertainty ellipse. Not surprisingly, the IMb point is very close to the reference CT66 one. These results mirror closely the range of variation of the u -quark distribution at $\sim 10^{-3}$ in Fig. 5 (with similar results for the d quark that is not shown), since the W/Z cross sections are dominated by the quark-antiquark annihilation process with the kinematic variable range $x \sim 10^{-3}$ and $Q \sim 80\text{--}90$ GeV. In particular, we see that the IMb quark line in Fig. 5a is extremely close to CTEQ6.6M (horizontal line) in this range.

The IMb prediction in Fig. 8(a) lies in the lower part of the CTEQ6.6 error ellipse, suggesting that the IMb ratio of the Z and W total cross section, $\sigma_{\text{tot}}(Z)/\sigma_{\text{tot}}(W)$, is lower than in the CTEQ6.6M case. This is again consistent with the observation that the IMb strange PDF $s(x, Q)$ is lower than the CTEQ6.6 one in the range of $x \sim 10^{-3}$ typical for W and Z production at the LHC. As noticed in Ref. [7], the ratio $\sigma_{\text{tot}}(Z)/\sigma_{\text{tot}}(W) \approx 0.1$ at the LHC, despite being well-constrained, is quite sensitive to the form of $s(x, Q)$. A smaller magnitude of $s(x, Q)$ thus results in a smaller $\sigma_{\text{tot}}(Z)/\sigma_{\text{tot}}(W)$ ratio.

4.4 Generalized rescaling variable in the GM scheme

The IM scheme results discussed above are sensitive to the choice of the parameter λ in the definition of ζ — an indication of its phenomenological origin. The choice of the scaling variable, involving powers of m/Q , is inherently an issue beyond the usual perturbative formalism. In fact, this ambiguity exists also in the GM scheme.

In principle, we could apply the proposed generalized rescaling variable ζ to the GM analysis (in place of the default ACOT- χ) as well. Will the GM formalism be stable with respect to variations of the λ parameter in ζ ? We expect the answer to be “yes”, since, as a PQCD theory including heavy-quark masses as the basic parameters of the Lagrangian, the GM formalism contains built-in compensation between the ζ dependence of the contributions from heavy-quark-initiated subprocesses and corresponding subtraction terms applied to gluon-fusion subprocesses at each order of α_s .

We have verified that this expectation indeed holds in practice. Specifically, in contrast to the large difference in the overall χ^2 of about 180 between the global fits IM χ ($\lambda = 0$) and IMb ($\lambda = 0.15$), the difference between the χ^2 values of two GM fits for these same λ values is only 12. The CTEQ6.6M PDF, corresponding to $\lambda = 0$, has a slightly better χ^2 than the GM fits with non-zero λ values, suggesting that the ACOT variable χ (motivated by the exact kinematics of the heavy-quark pair production in the gluon fusion process) does the best job of all in the GM case. The GM PDFs for λ as high as 0.4 remain within the band of the CTEQ6.6 PDF uncertainty, while the IM fit with $\lambda = 0.4$ is strongly disfavored. Predictions for the LHC W and Z cross sections based on GM fits with $\lambda < 0.3$ lie within the CTEQ6.6 PDF error ellipse, as illustrated by Fig. 8(b). Sensitivity of GM cross sections to λ is clearly reduced in comparison to the IM calculation.

5 Concluding Remarks

For many years, the ZM variable-flavor number factorization scheme has given a high-quality description of existing global hard-scattering data and provided predictions for a wide range of high-energy processes. Even though by now the GM scheme has superseded the ZM scheme as the more precise formalism, the ZM scheme still has a lot of appeal for practical reasons. It continues to be used in most phenomenological calculations. For this reason, we carry out the present study to lay out more explicitly the approximations and inconsistencies inherent in the conventional implementation of the ZM scheme. We show how these inconsistencies, due to the *ad hoc* imposition of the heavy-quark mass thresholds on the zero-mass QCD theory, can be corrected by a more careful physical treatment of the heavy-flavor final states, while preserving the simplicity of the ZM hard matrix elements. Our proposed intermediate-mass (IM) calculational scheme can be considered either as *improved ZM formulations* with GM kinematics of final states, or *simplified GM formulations* with ZM hard matrix elements.

The key element that makes the IM scheme useful is the introduction of a flexible rescaling variable ζ that generalizes the mass-dependent rescaling variable χ [18] that has already

been adopted by the latest global analyses in the GM scheme. The ζ variable effectively implements kinematic mass threshold constraints in heavy-quark production processes, while minimizing unintended effects away from the physical threshold region in a smooth, controlled way by a parameter λ , cf. Sec. 3.1. This allows us to systematically investigate how the conventional ZM scheme can be improved while keeping the simple, well-known, ZM matrix elements.

We demonstrated that global analysis carried out in the IM scheme can approximate the GM scheme results quite well, both in terms of the resulting PDFs, and in terms of typical physics predictions at the Tevatron and the LHC. The IM scheme can play a useful role in bringing the existing NLO analyses based on ZM hard matrix elements closer to the GM formulation, even without the full implementation of heavy-quark mass effects. Dependence of the IM predictions on the form of the effective rescaling variable underlines the phenomenological nature of this approach. Although this dependence in principle also arises in the GM formalism, we have demonstrated that it is less pronounced than in the phenomenological IM formulation. Thus, this additional source of theoretical uncertainty hardly affects what we know about the GM formalism – except that, perhaps, it should be added to the other sources of theoretical errors, such as scale dependence, when assessing the uncertainty of the GM theoretical results.

Acknowledgments WKT would like to thank Robert Thorne for useful discussions related to this subject during collaborative work on Ref. [9], and for cogent remarks on an early draft of this paper. We thank Paul Thompson for a critical reading of the manuscript and many helpful suggestions for improvements of the presentation. This work is supported by the National Science Foundation (USA) under the grant PHY-0354838. PMN is partly supported by the U.S. Department of Energy under grant DE-FG02-04ER41299, and by Lightner-Sams Foundation.

References

- [1] D. Amati, R. Petronzio and G. Veneziano, Nucl. Phys. B **140**, 54 (1978); *ibid.*, B **146**, 29 (1978); S. B. Libby and G. Sterman, Phys. Rev. D **18**, 3252 (1978); *ibid.*, D **18**, 4737 (1978); A. H. Mueller, Phys. Rev. D **18**, 3705 (1978); R. K. Ellis, H. Georgi, M. Machacek, H. D. Politzer and G. G. Ross, Nucl. Phys. B **152**, 285 (1979); G. Bodwin, Phys. Rev. D **31**, 2616 (1985); J. C. Collins, D. E. Soper, and G. Sterman, Nucl. Phys. B **261**, 104 (1985); *ibid.*, B **308**, 833 (1988).
- [2] W. Bernreuther and W. Wetzel, Nucl. Phys. B **197**, 228 (1982) [Erratum-*ibid.* B **513**, 758 (1998)]; W. J. Marciano, Phys. Rev. D **29**, 580 (1984).

- [3] J. C. Collins and W.-K. Tung, Nucl. Phys. B **278**, 934 (1986); R. M. Barnett, H. E. Haber, and D. E. Soper, Nucl. Phys. B **306**, 697 (1988); F. I. Olness and W.-K. Tung, Nucl. Phys. B **308**, 813 (1988).
- [4] M. Aivazis, J. C. Collins, F. Olness and W.-K. Tung, Phys. Rev. **D50** (1994) 3102.
- [5] J. C. Collins, Phys. Rev. D **58**, 094002 (1998) [arXiv:hep-ph/9806259].
- [6] W.-K. Tung, H.-L. Lai, A. Belyaev, J. Pumplin, D. Stump and C.-P. Yuan, JHEP **0702** (2007) 053 [arXiv:hep-ph/0611254].
- [7] P. M. Nadolsky, H.-L. Lai, Q.-H. Cao, J. Huston, J. C. Pumplin, D. R. Stump, W.-K. Tung, and C.-P. Yuan, Phys. Rev. D **78**, 013004 (2008).
- [8] A. D. Martin, W. J. Stirling, R. S. Thorne and G. Watt, arXiv:0901.0002 [hep-ph].
- [9] R. S. Thorne and W.-K. Tung, arXiv:0809.0714 [hep-ph].
- [10] J. Pumplin, D. R. Stump, J. Huston, H.-L. Lai, P. Nadolsky and W.-K. Tung, JHEP **0207**, 012 (2002) [arXiv:hep-ph/0201195].
- [11] D. Stump, J. Huston, J. Pumplin, W.-K. Tung, H.-L. Lai, S. Kuhlmann and J. F. Owens, JHEP **0310**, 046 (2003) [arXiv:hep-ph/0303013].
- [12] S. Alekhin, Phys. Rev. D **68** (2003) 014002 [arXiv:hep-ph/0211096]; C. Adloff *et al.* [H1 Collaboration], Eur. Phys. J. C **30**, 1 (2003) [arXiv:hep-ex/0304003]; S. Chekanov *et al.* [ZEUS Collaboration], Eur. Phys. J. C **42**, 1 (2005) [arXiv:hep-ph/0503274]; S. Alekhin, K. Melnikov, and F. Petriello, Phys. Rev. D **74**, 054033 (2006) [arXiv:hep-ph/0606237]; J. Blumlein, H. Bottcher and A. Guffanti, Nucl. Phys. B **774**, 182 (2007) [arXiv:hep-ph/0607200]; H1 and ZEUS Collaborations Contributions to the Proceedings of The XXXIV International Conference on High Energy Physics, ICHEP08, Philadelphia, USA, H1prelim-08-045, ZEUS-prel-08-003; B. C. Reisert [ZEUS Collaboration], arXiv:0809.4946 [hep-ex]; R. D. Ball *et al.* [NNPDF Collaboration], arXiv:0808.1231 [hep-ph]; K. J. Eskola, H. Paukkunen, and C. A. Salgado, JHEP **0807** (2008) 102.
- [13] J. A. M. Vermaseren, A. Vogt, and S. Moch, Nucl. Phys. B **724**, 3 (2005) [arXiv:hep-ph/0504242]; C. Anastasiou, L. J. Dixon, K. Melnikov, and F. Petriello, Phys. Rev. Lett. **91**, 182002 (2003) [arXiv:hep-ph/0306192]; Phys. Rev. D **69**, 094008 (2004) [arXiv:hep-ph/0312266].
- [14] E. Laenen, S. Riemersma, J. Smith and W. L. van Neerven, Nucl. Phys. B **392**, 162 (1993); S. Riemersma, J. Smith and W. L. van Neerven, Phys. Lett. B **347**, 143 (1995) [arXiv:hep-ph/9411431]; B. W. Harris and J. Smith, Nucl. Phys. B **452**, 109 (1995) [arXiv:hep-ph/9503484]; M. Buza, Y. Matiounine, J. Smith and W. L. van Neerven,

- Eur. Phys. J. C **1**, 301 (1998) [arXiv:hep-ph/9612398]; I. Bierenbaum, J. Blumlein and S. Klein, Phys. Lett. B **672**, 401 (2009) [arXiv:0901.0669 [hep-ph]].
- [15] H.L. Lai, J. Huston, S. Kuhlmann, J. Morfin, F. Olness, J. F. Owens, J. Pumplin, W.K. Tung Eur. Phys. J. C **12**, 375 (2000) [arXiv:hep-ph/9903282].
 - [16] S. Kretzer, H.-L. Lai, F. I. Olness and W.-K. Tung, Phys. Rev. D **69**, 114005 (2004) [arXiv:hep-ph/0307022].
 - [17] R. M. Barnett, Phys. Rev. Lett. **36**, 1163 (1976); T. Gottschalk, Phys. Rev. D **23**, 56 (1981).
 - [18] W. K. Tung, S. Kretzer and C. Schmidt, J. Phys. G **28**, 983 (2002) [arXiv:hep-ph/0110247].
 - [19] C. Adloff *et al.* [H1 Collaboration], Phys. Lett. B **528**, 199 (2002) [hep-ex/0108039].
 - [20] A. Aktas *et al.* [H1 Collaboration], Eur. Phys. J. C **40**, 349 (2005) [hep-ex/0411046].
 - [21] A. Aktas *et al.* [H1 Collaboration], Eur. Phys. J. C **45**, 23 (2006) [hep-ex/0507081].
 - [22] J. Breitweg *et al.* [ZEUS Collaboration], Eur. Phys. J. C **12**, 35 (2000) [hep-ex/9908012].
 - [23] S. Chekanov *et al.* [ZEUS Collaboration], Phys. Rev. D **69**, 012004 (2004) [hep-ex/0308068].
 - [24] M. Goncharov *et al.* [NuTeV Collaboration], Phys. Rev. D **64**, 112006 (2001) [hep-ex/0102049].
 - [25] M. Spira, arXiv:hep-ph/9510347.
 - [26] M. Spira, Fortsch. Phys. **46**, 203 (1998) [arXiv:hep-ph/9705337].
 - [27] J. L. Diaz-Cruz, H.-J. He, and C.-P. Yuan, Phys. Lett. B **530**, 179 (2002) [arXiv:hep-ph/0103178].
 - [28] C.-P. Yuan and collaborators, unpublished.